Research Article

Experimental Investigation on the Energy Consumption Difference between the Dynamic Impact and the Drilling Tests of Rocks

Shoudong Xie [1,2,3] **Mingjian Huang,** [4,5] **Junji Lu,** [4] **Wang Xi,** [6] **and Zhenyang Xu** [7]

[1]*State Key Laboratory of Mining Response and Disaster Prevention and Control in Deep Coal Mines,*
Anhui University of Science and Technology, Huainan, Anhui 232001, China
[2]*School of Civil Engineering and Architecture, Anhui University of Science and Technology, Huainan, Anhui 232001, China*
[3]*Hongda Blasting Engineering Group Co., Ltd., Changsha, Hunan 410011, China*
[4]*School of Resources and Safety Engineering, Central South University, Changsha 410083, China*
[5]*Hunan Lianshao Construction Engineering (Group) Co., Ltd., Changsha 410011, China*
[6]*Fujian Xinhuadu Engineering Co., Ltd., Xiamen 361000, China*
[7]*School of Mining Engineering, University of Science and Technology Liaoning, Anshan 114051, China*

Correspondence should be addressed to Zhenyang Xu; 463411533@qq.com

The split Hopkinson pressure bar (SHPB) technique and various drilling tests were performed on three types of lithologies (granite and cyan and red sandstone) to understand the variation in energy consumption (EC) of the different methods used for rock crushing. The dynamic behavior of rocks was analyzed based on the dynamic stress-strain curve, the peak stress, the energy, and the failure mode for the SHPB test, while the drilling curve, the influence of the drilling pressure (DP) and the revolution speed (RS) on the drilling speed (DS) were analyzed for the drilling test. Additionally, the EC difference was compared based on the EC required to break a single unit volume of rock. The obtained results indicate that the sensitivity of the dynamic strength of rocks with different lithologies to strain rate is different and that the higher the uniaxial compressive strength is, the more sensitive it is. Additionally, the strengthening of the peak stress is more pronounced with the increase in the strain rate. The energy utilization efficiency (EUE) of the SHPB test sample has a positive correlation with the strain rate. Moreover, the typical drilling process can be divided into the initial drilling and stable drilling stages, with the DS during the stable drilling stage being lower than that during the initial drilling stage. The DP and the RS have a linear positive correlation with the DS, with the influence of the DP on the DS being more obvious. Finally, the EC during the drilling process is higher than the EC during the SHPB technique.

1. Introduction

The rock mass in deep underground engineering constructions is affected by the dynamic load [1–4], which derives from impact, blasting, drilling, earthquakes, and other processes [5–10]. Therefore, understanding the crushing mechanism and the failure behavior of rocks under dynamic load is of great importance for the stability evaluation of rock mass engineering and disaster prevention [11, 12]. The dynamic mechanical parameters of rocks are usually determined by the split Hopkinson pressure bar

(SHPB) test device [13–15]. However, in practice, the dynamic mechanical parameters of rocks obtained by the traditional dynamic mechanical test require the preparation of rock samples, which cannot be applied for the real-time analysis of rock properties [16–18]. Therefore, real-time performance is usually poor, the statistical calculation of the parameters is complex, and the working cycle is lengthy. Additionally, several studies have shown that there is a good correlation between the drilling parameters and the rock mechanical parameters. The drilling test can be used for the evaluation of rock properties, while the rock mechanical

parameters can be obtained in real-time during drilling. Thus, the collected parameters can be visualized on-site during the drilling operations [19, 20].

In the last years, drilling tests have been widely used in the quantitative evaluation of rock mechanical parameters [21, 22]. For example, the properties of rocks were analyzed by applying two essential drilling parameters: the intrinsic energy and the drilling rate [23]. A new test system was built to study the drilling efficiency of the bit to optimize the accuracy of drilling and obtain more accurate drill bit data [24]. The field and laboratory drilling tests on rocks were performed to obtain a preliminary quantitative evaluation of rock properties [25–27]. In the above studies, the authors used test parameters that were correlated with the rock properties and proposed the corresponding characterization equations. Additionally, a multifunctional digital rock drilling test system was developed and used to perform digital drilling tests on intact, broken, and grouted rock masses with the purpose of accurately measuring the rock strength parameters for underground constructions [28].

A correlation equation between the drilling parameters and the rock strength was established using the revolution speed and the bit weight from drilling test data [29]. Additionally, the test results indicate that it is more reliable to estimate rock strength using the parameters obtained from the drilling test. The drilling test has been introduced into practical engineering investigations; the results show a better and more accurate measurement of rock strength and other parameters in practical applications [30, 31]. A method to obtain mechanical indexes of rocks was proposed by inversing the drilling parameters of the digital drilling rig. Another method also was proposed to obtain the rock mechanics parameters by inversing the drilling parameters, and the effectiveness of the proposed method was verified [32]. Additionally, the influence of the drilling parameters (including the borehole diameter and borehole number) on the behavior of rock mechanics through experiments was studied, which provided information for optimizing the drilling parameters [33]. Moreover, the mathematical relationship between the drilling parameters and the rock mass mechanical indexes during the process of rotary penetration was established through the on-site rock mass mechanical parameters probe and determined the strength of soil and soft rocks [34].

In summary, extra attention has been paid to the relationship between the drilling parameters and the rock mechanics parameters, and less consideration has been given to the difference in energy consumption characteristics between the drilling and the dynamic impact of rocks. However, for bench blasting operations in open-pit mines, it is preferable to obtain the energy dissipation characteristics of the rock mass through the drilling parameters because the mechanism of rock crushing by drilling and dynamic impact is quite different. Therefore, it is necessary to study the energy dissipation characteristics of the previously mentioned methods used for rock crushing. In this article, the dynamic impact and drilling tests were performed on three types of rocks with different lithologies, and the energy dissipation characteristics during these processes were

discussed. This study aims to provide information for guiding and optimizing the blasting operations design by analyzing the bench borehole drilling data from an open-pit mine.

2. Materials and Methods

2.1. Materials. Dynamic impact and drilling tests were performed on three types of lithologies (granite, cyan sandstone, and red sandstone). The samples were collected in the Shandong province, China, and processed into cylinders (the diameter and the height are both equal to 50 mm), as shown in Figure 1(a). Additionally, Figure 1(b) indicates the mineralogical composition deduced from the X-ray diffraction of the three types of samples. Among these, the quartz content in the red sandstone has the highest value (77.8%). The P-wave velocity, the uniaxial compressive strength (UCS), and the elastic modulus of the three types of samples were measured before the dynamic impact tests. In terms of strength, the granite sample has the highest strength. The red sandstone shows the lowest strength, which is approximately 43.3% of the cyan sandstone strength. Table 1 highlights the specific values of the basic mechanical parameters.

2.2. Experimental System

2.2.1. SHPB Apparatus. Figure 2(a) illustrates the SHPB test system, and Figure 2(b) reveals the schematic diagram of the system. The system is equipped with an axial prepressure and a confining pressure loading device to perform a dynamic-static combined loading test. The sample failure process is captured by a high-speed photography system. The cylindrical punch (diameter is equal to 50 mm), the incident bar, the transmission bar, and the absorption bar of the test device are made up of 50Cr steel, Young's modulus is 240 GPa, the density is 7800 kg/m^3, the P-wave velocity in the bar is 5580 m/s, and the wave impedance is 4.35×10^7 MPa/s. The rock strain signals were obtained by an LK2109A superdynamic strain gauge and an LK2400 high-speed data collector. During the test, the BC-202 dual-channel detonation velocity meter was used to measure the velocity of the punch. The constant velocity impact was carried out by controlling the pressure of the high-pressure chamber, and the velocity of the punch was modified by adjusting the impact pressure or by reducing the depth of the punch into the chamber to achieve the required impact velocity.

2.2.2. Drilling Test Device. Figure 3 shows the drilling test device, which includes the revolution speed (RS) control, the pressure measurement, and the drilling depth measurement systems. The instrument can register the dynamic control of the drilling pressure (DP) and the speed (DS). The pressure measurement device can display the pressure variation on the sample and the drilling depth of the bit in real-time. In this article, a 6 mm alloy triangular twist bit was used; in
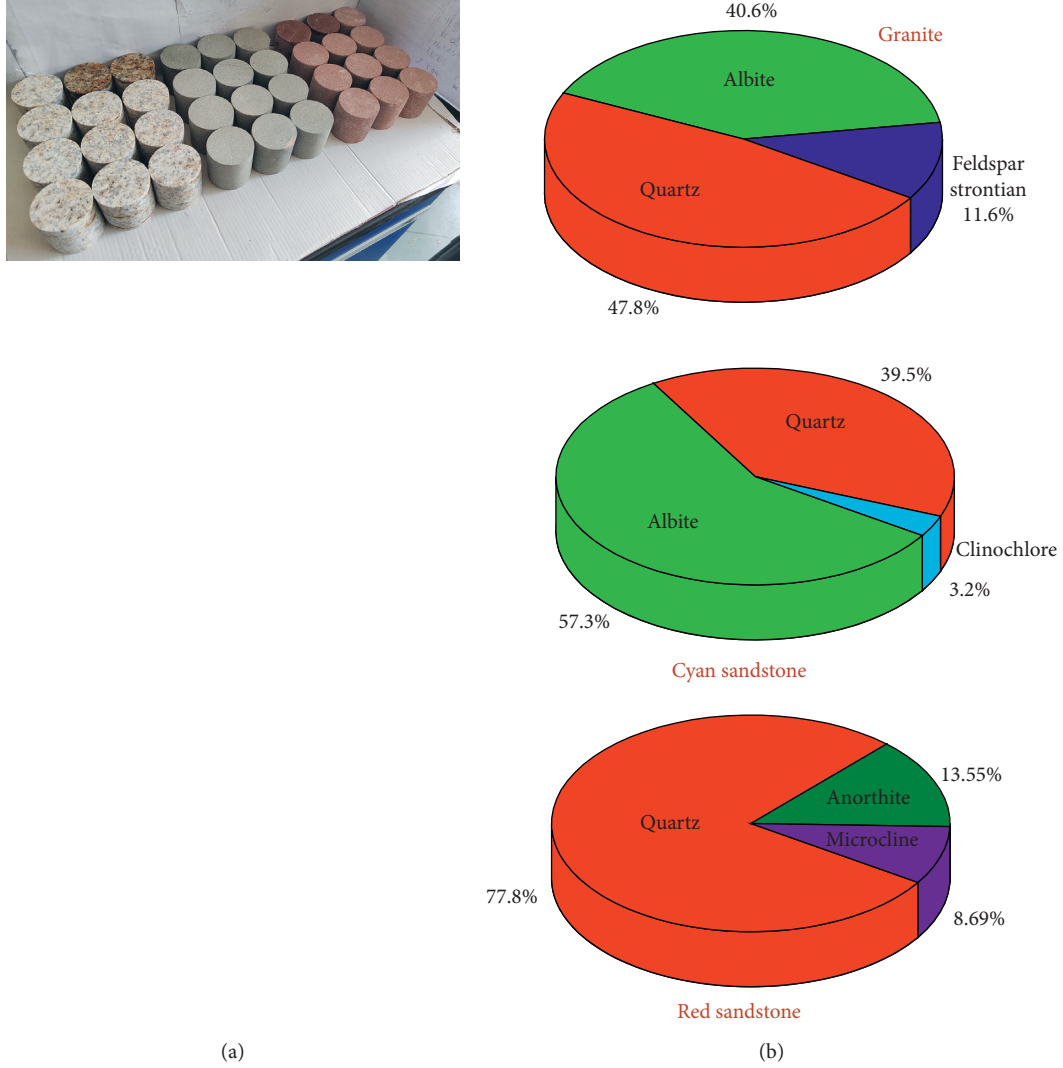
FIGURE 1: Photographs of (a) the test samples (granite, cyan sandstone, and red sandstone) and (b) their mineralogical composition.

TABLE 1: Physical and mechanical parameters of specimen.

Specimen	P-wave velocity (m/s)	UCS (MPa)	Elastic modulus (GPa)
Granite (G)	3585.3	103.8	83.5
Cyan sandstone (S1)	2526.3	73.0	23.7
Red sandstone (S2)	2369.3	31.6	15.6

order to reduce the influence of bit wear on the test results, a new bit was used for each test. The drilling tests on granite, cyan sandstone, and red sandstone under different DPs and different RSs were carried out by control variable method. The variation process of the DS with the DP and the RS was measured.

2.3. Data Processing for the SHPB Test.

For the SHPB test, the three-wave method [35] is one of the most used methods for processing test data. The following equation is the calculation formula of stress, strain, and strain rate in the sample:

$$
\begin{cases}
\sigma_s = \dfrac{A_0 E_0}{2A_s} (\varepsilon_I + \varepsilon_R + \varepsilon_T), \\[2mm]
\varepsilon_s = \dfrac{C_0}{l_s} \displaystyle\int_0^t (\varepsilon_I - \varepsilon_R - \varepsilon_T)\,dt, \\[2mm]
\dot{\varepsilon}_s = \dfrac{C_0}{l_s} (\varepsilon_I - \varepsilon_R - \varepsilon_T),
\end{cases}
\tag{1}
$$

where σ_s, ε_s, and $\dot{\varepsilon}_s$ are the dynamic compressive stress, the strain, and the strain rate, respectively; A_0, E_0, and C_0 are the
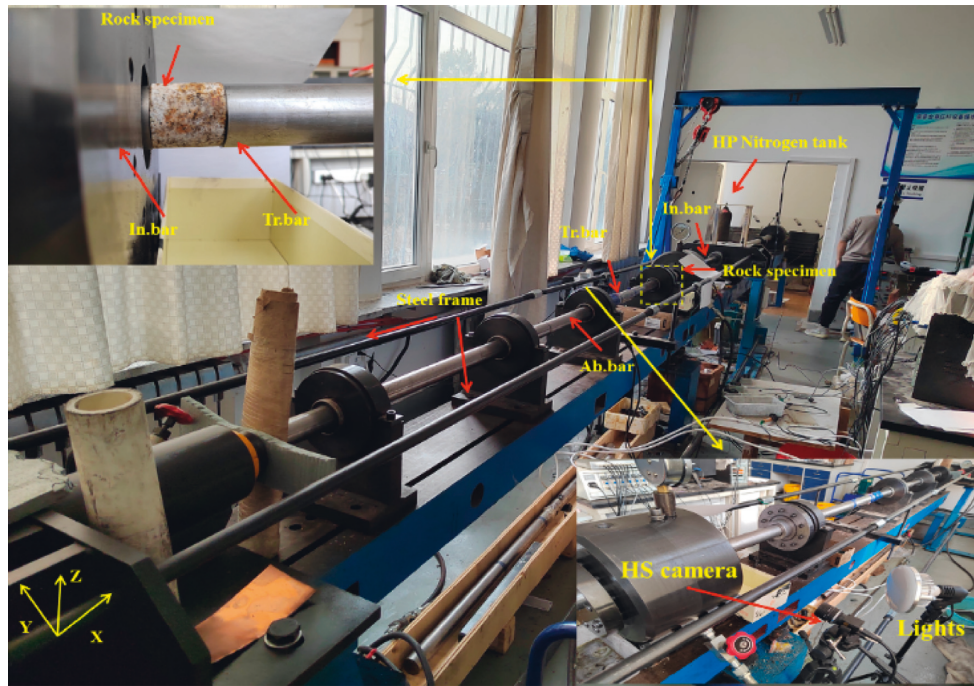
(a)
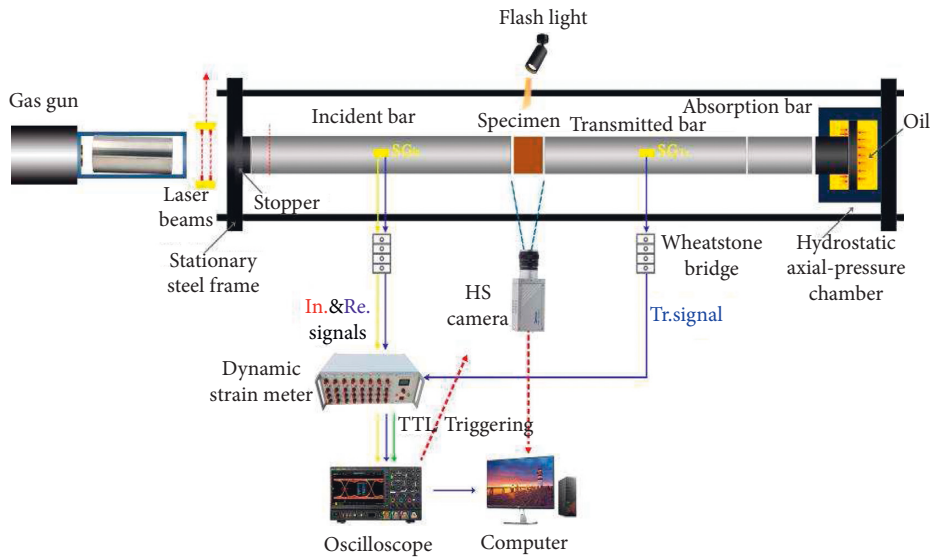
(b)

Figure 2: The SHPB test system: (a) a photograph of the SHPB device and (b) a schematic diagram of the SHPB system.

cross-sectional area, the elastic modulus, and the P-wave velocity of the elastic bars, respectively; A_s and l_s are the cross-sectional area and the length of the specimen; and ε_I, ε_R, and ε_T are incident, reflected, and transmitted wave signals, respectively.

2.3.1. Dynamic Stress Equilibrium. Whether the dynamic stress is balanced or not is an important premise to measure the effectiveness of the dynamic impact test, which can be verified by the time-history curves of the waveform. It can be

observed from Figure 4 that the transmitted wave has a high degree of concordance with the sum of the incident and reflected waves; thus, it satisfies the premise of dynamic stress balance, which means that the dynamic impact test of the rock is effective.

2.3.2. Calculation of Energy. For the test data, the dynamic strength of the rock represents the peak stress. Additionally, the incident energy (W_i), the reflected energy (W_r), and the transmitted energy (W_t) of the stress waves can be
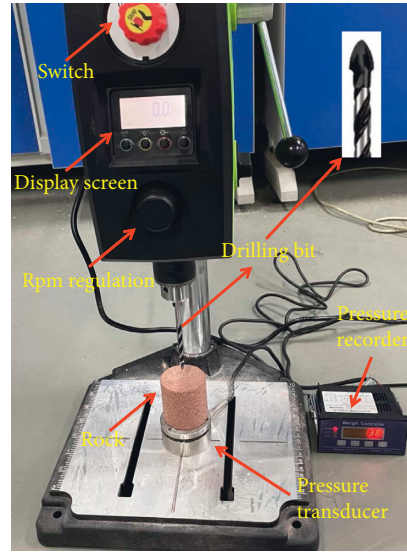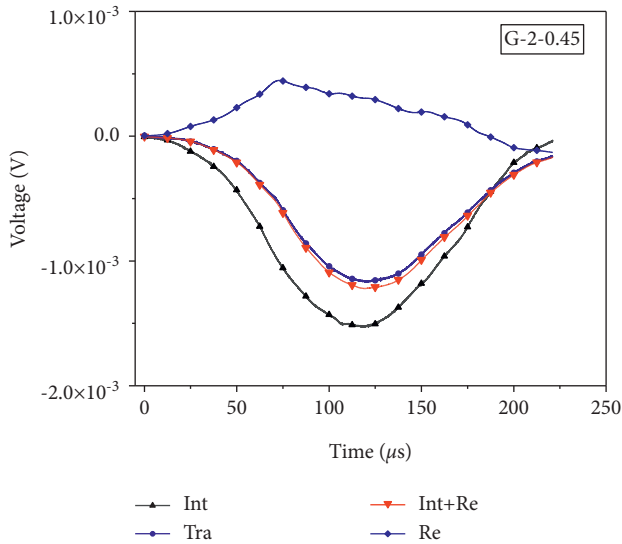
FIGURE 3: Rock drilling test device.

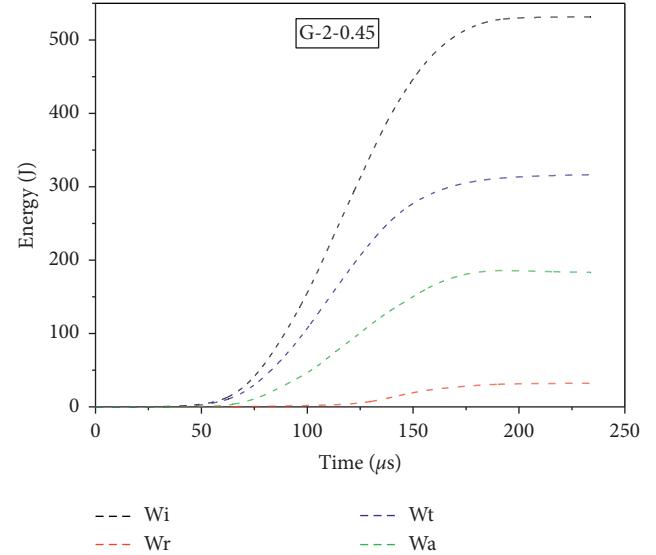FIGURE 4: Dynamic stresses on both ends of the granite specimen.

FIGURE 5: Energy evolution of the granite sample (G-2-0.45).

determined using equations (2)–(4) [36]. Moreover, based on the conservation of energy, the absorbed energy (W_a) by rock specimens during impact can also be determined using equation (5). Figure 5 shows the variation of the four types of energies for the specimen G-2-0.45 during the impact test. The variation process of all energies is the same, which initially increases uniformly and then becomes stable. Overall, the generated energies decrease in the following order: from W_t to W_a and W_r, respectively. Additionally, the parameter (W_a/W_i) can be used to evaluate the energy utilization efficiency. In general, the energy absorbed by the brittle material mainly consists of three parts: the fracture energy (which produces new cracks), the heat and acoustic energy, and the kinetic energy of the blocks. The last two parts have a small contribution and can be ignored in calculations.

$$W_i = C_0 A_0 E_0 \int_0^\tau \varepsilon_I^2 d, \tag{2}$$

$$W_r = C_0 A_0 E_0 \int_0^\tau \varepsilon_R^2 dt, \tag{3}$$

$$W_t = C_0 A_0 E_0 \int_0^\tau \varepsilon_T^2 dt, \tag{4}$$

$$W_a = W_I - W_R - W_T. \tag{5}$$

2.4. Experimental Design. In this study, SHPB dynamic impact and drilling tests were performed on three common rock lithologies (granite, cyan sandstone, and red sandstone). The impact failure at different strain rates was

registered by setting different gas pressures for the SHPB tests, and the specific values of each test sample are shown in Table 2.

Four different pressures were set for each lithology, and the specific pressure gradient was determined by performing measurements before the official analyses. Regarding the drilling tests, the drilling parameters were obtained by drilling without any lateral constraints. Four groups of drilling tests with different RSs were set up based on different lithologies. Additionally, four different DPs were selected for each group. Table 3 illustrates the specific values in detail. Since the granite samples are characterized by high strength values, the RSs and the DPs values are larger accordingly, while the drilling parameters of the cyan and the red sandstones are consistent. Additionally, the DS was obtained by recording the bit footage data during the drilling process.

3. Results and Discussion

3.1. Dynamic Properties

3.1.1. Mechanical Behavior. According to the data processing method described in Section 2.3, the maximum strain rate and the peak stress of all the test samples were calculated by processing the impact test data of granite, cyan sandstone, and red sandstone samples under different strain rates, as shown in Table 2. After that, three test samples with similar strain rates were selected to analyze the characteristics of dynamic stress-strain curves. Figure 6 illustrates the typical stress-strain curves of the analyzed samples. It is observed that when the strain rates are almost similar, the overall form of the dynamic stress-strain curves of the three types of samples is rather different. The granite samples are characterized by the highest peak stress values and a curve before the peak stress, which resembles the form of an inverted parabola. The turning point between the elastic stage and the plastic stage is not clear. Additionally, the overall variation process (which belongs to the typical class II curve) can be divided into four stages: elastic stage, strain hardening stage, strain softening stage, and rebound stage. Among these, the stress in stage III decreases with the increase of the strain and corresponds to the absorption of energy. Moreover, stage IV corresponds to the release of the elastic energy, and the elastic modulus of the rebound stage is basically the same as that of the elastic stage.

Compared with the granite, the stress-strain curves of the cyan sandstone and the red sandstone have closer values. However, the curve of the cyan sandstone before the elastic stage is concave, with an obvious pore closure process, while the red sandstone enters directly into the elastic stage. Overall, the plastic deformation of the cyan sandstone and the red sandstone before the peak stress is more distinct. The strain strengthening effect is weak, which means that the larger strain increment corresponds to the smaller stress increment. For the cyan sandstone, the postpeak stress softening stage has a short duration, and the elastic modulus of the elastic stage is almost the same as that of the plastic stage. The rebound strain is also large, which returns to the strain corresponding to the peak stress. Finally, for the red

sandstone with the lowest strength values, the postpeak strain weakening stage has a longer duration and the peak strain is the largest. Additionally, the rebound deformation is smaller during the rebound stage, which points out that its plastic deformation is the most pronounced.

Figure 7 shows the various processes of the peak stress of all the test samples based on the strain rate. For the samples with similar lithologies, the peak stress has a linear correlation with the strain rate, and the appropriate degree of the linear fitting is greater than 0.8. The dynamic strength of the granite samples indicates the biggest increase with the increase of the strain rate.

Additionally, the positive steepness of the slope has the greatest value compared to the other slopes, while that of the red sandstone is the lowest. Although the gas pressure derived from the impact test for the granite samples is relatively high, the variation range of the strain rate is small, while the strain rate distribution range of the cyan sandstone is relatively wide. Overall, the strength of the red sandstone has the lowest values, while the strength of the granite indicates the highest values. However, when the strain rate of the cyan sandstone is large enough, the peak stress can reach values close to those of the granite. The ratios (dynamic increase factor, DIF, as listed in Table 2) of the dynamic strength of the rock to the UCS can be used to characterize the strain rate strengthening effect. It can be observed from Table 2 that the DIF values of the granite are low, with an average value equal to 3.0, while those of the cyan sandstone and the red sandstone are 9.1 and 8.8, respectively. Thus, the granite sample has the lowest sensitivity to the strain rate effect, while the other two lithologies with lower strength values have the closest response to the strain rate effect, which is strong in both cases.

3.1.2. Energy Dissipation. According to the energy calculation formula in subchapter 2.3.2, the W_i, W_r, W_t, and W_a parameters were calculated, as listed in Table 2. Overall, for the samples with the same lithology, the larger strain rate corresponds to larger W_i values. Additionally, there is no direct relationship between the values of the W_r and the W_t with the strain rate. When the strain rate is larger, W_t may also be smaller, as is the case for S1-1-0.4 and S2-1-0.3. Moreover, the relationship between W_i and the sum of W_r and W_t can reflect the energy absorption state of the sample. Figure 8 represents the scatter plot of the $(W_r + W_t)$ sum versus W_i. The diagonal line is considered as the dividing line of energy absorption, which means that the sample has energy absorption if it is located under this line, while the distance between the scatter points and the diagonal line represents how much of the energy is being absorbed. That is, the closer the distance, the weaker the energy absorption. Therefore, the three types of test samples will absorb energy under dynamic loading, while the energy absorption capacity of the red sandstone, the granite, and the cyan sandstone is improved.

The energy utilization efficiency (EUE) of different samples can be measured using the W_a/W_i ratio. Figures 9(a) and 9(b) show the EUE variation with the increase of the

TABLE 2: Dynamic mechanical parameters of different specimens for SHPB test.

Specimen no.	Strain rate (s^{-1})	Peak stress (MPa)	DIF[*]	W_i (J)	W_r (J)	W_t (J)	W_a (J)	η (MPa)	W_a/W_i (%)
G-2-0.35[*]	78.0	158.0	1.9	368.2	102.7	210.3	32.9	0.084	8.9
G-2-0.38	96.1	244.6	2.9	402.7	163.1	212.3	46.3	0.118	11.5
G-2-0.45	99.6	266.4	3.2	482.9	187.6	222.9	72.4	0.184	15.1
G-2-0.5	107.0	322.6	3.9	519.4	84.2	376.3	117.9	0.300	22.7
S1-1-0.2	62.1	127.5	5.4	177.6	54.0	100.9	25.9	0.066	14.6
S1-1-0.25	118.7	190.1	8.0	235.3	69.8	118.9	46.6	0.119	19.8
S1-1-0.3	159.6	239.0	10.1	289.4	107.9	119.8	61.7	0.157	25.8
S1-1-0.4	194.6	301.4	12.7	407.4	180.5	88.9	140.5	0.358	34.5
S2-1-0.23	69.9	122.3	7.8	206.3	94.9	88.5	22.9	0.058	11.1
S2-1-0.25	86.0	133.0	8.5	243.9	116.6	96.1	31.2	0.079	12.8
S2-1-0.27	111.3	141.5	9.1	250.3	130.8	82.2	37.3	0.095	14.9
S2-1-0.3	133.5	153.3	9.8	265.2	142.6	68.6	54.0	0.138	20.4

[*]Note: G means granite, S1 means cyan sandstone, S2 means red sandstone, 0.35 means gas pressure; DIF means dynamic increase factor, which is the ratio of dynamic peak stress to UCS.

TABLE 3: Drilling test parameters of different samples.

Item	R[*] (r/min)	P (N)	v (mm/s)	Item	R (r/min)	P (N)	v (mm/s)	Item	R (r/min)	P (N)	v (mm/s)
		250	0.49			30	0.18			30	0.21
		300	0.92			40	0.21			40	0.32
	1400	350	1.22		700	50	0.28		700	50	0.42
		400	1.53			60	0.37			60	0.53
		250	0.88			30	0.19			30	0.40
		300	1.12			40	0.23			40	0.46
	1600	350	1.32		900	50	0.31		900	50	0.63
		400	1.64			60	0.39			60	0.80
Granite		250	1.12	Cyan sandstone		30	0.21	Red sandstone		30	0.45
		300	1.27			40	0.27			40	0.54
	1800	350	1.43		1100	50	0.32		1100	50	0.77
		400	1.76			60	0.41			60	0.91
		250	1.32			30	0.24			30	0.52
		300	1.43			40	0.28			40	0.65
	2000	350	1.59		1300	50	0.35		1300	50	1.02
		400	1.88			60	0.44			60	1.15

[*]Note: R, P, and v represent revolution speed, drilling pressure, and drilling speed, respectively; additionally, the drilling speed was obtained under the bit wear without counting.
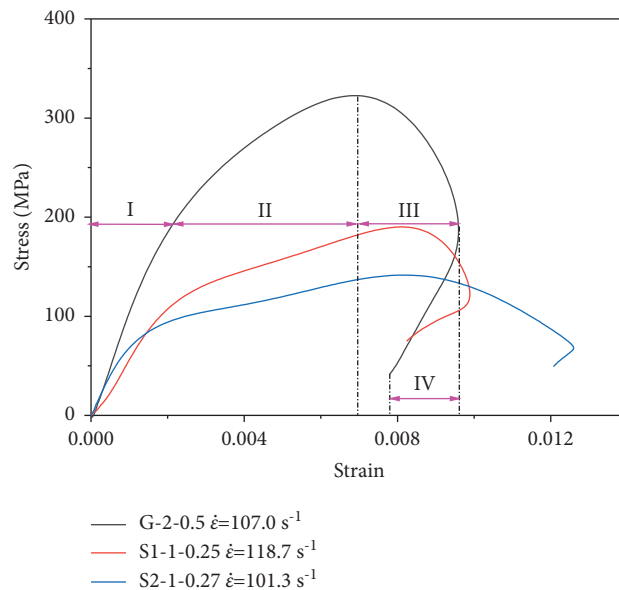

FIGURE 6: Typical dynamic stress-strain curves of granite, cyan sandstone, and red sandstone samples.
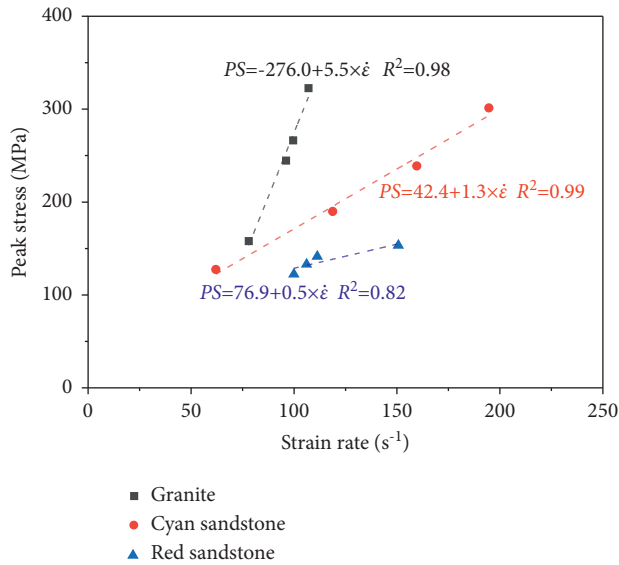
FIGURE 7: Relationship between the peak stress and the strain rate for the different types of rocks.
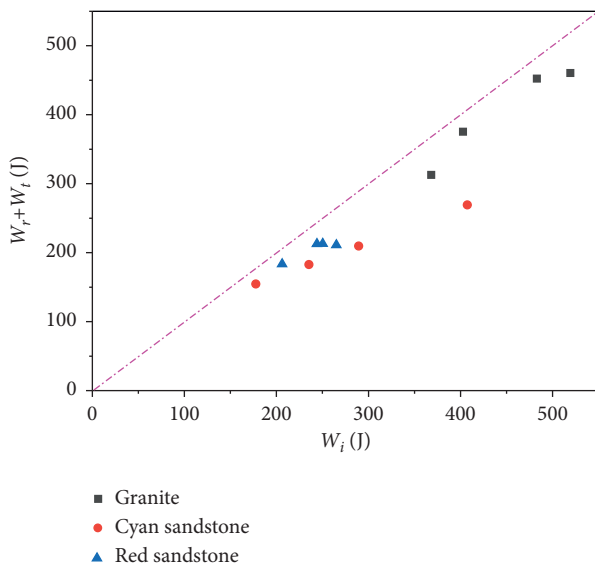

FIGURE 8: Variations of unused energy of different types of rocks.

incident energy and the strain rate, respectively. It can be seen from Figure 9(a) that for samples with different lithologies, greater values of the incident energy lead to higher EUE values. The incident energy of the granite is primarily high, while the EUE ranges between 8.9% and 22.7%, with an average value of 14.6%. However, the incident energy of the red sandstone is mainly low, with an average EUE value equal to 14.8%. Although the maximum incident energy of the cyan sandstone is lower than the values of the granite, its EUE has a wider distribution range (14.6%–34.5%) and contains the highest values, with an average of 23.7%. The EUE of the granite and the cyan sandstone shows a linear correlation with the incident energy, while the red sandstone has values that form a quadratic curve. It can be observed from Figure 9(b) that the

EUE and the strain rate also indicate a positive correlation, and this relationship can be characterized in the form of a quadratic curve. For the granite samples, the variation process of the quadratic curve has the steepest slope, suggesting that the EUE is associated with the modifications in strain rate, and the increase of the strain rate in a specific range will reduce the EUE. On the other hand, the EUE of the cyan sandstone and the red sandstone is less susceptible to any modifications of the strain rate, with the EUE of the cyan sandstone being higher than the values of the red sandstone. For the three different lithological samples, when the strain rate is equal to $100\,s^{-1}$, then the EUE values decrease in the following order: cyan sandstone, granite, and red sandstone. However, with the increase of the strain rate (such as $110\,s^{-1}$), then the EUE of the granite will increase above the cyan sandstone values.

3.1.3. Failure Patterns. The failure mode of the sample and the fragmentation characteristics of the fragments can reflect, to some degree, the failure mechanism of the rock. The impact-derived fragments were sieved through the standard mesh strainers (including five sizes: 5 mm, 2 mm, 1 mm, 0.5 mm, and 0.075 mm), and the classification of specific particle sizes at different strain rates is illustrated in Figure 10. Thus, the increment of the strain rate will aggravate the crushing degree of the sample, which is expressed by the increase in the number of fragments with particle sizes greater than 5 mm, the decrease in the number of large blocks, and smaller sized fragments.

For the cyan sandstone, the influence of the strain rate on the degree of fragmentation is particularly obvious. As shown in Figure 10(b), when the strain rate has the smallest values, the specimen (S1-1-0.2) displays minor damage at its edges. With the increase of the strain rate, the failure area of the specimen gradually expands, and the influence depth of the inverted cone failure gradually deepens (S1-1-0.25 and S1-1-0.3) until it is completely broken. Due to its high-pressure values, the failure of the whole granite sample is relatively serious. Thus, the sample G-2-0.5 is mostly entirely crushed, while the other samples comprise large blocks. At the same time, the strain rate effect of the red sandstone failure is also noticeable. When the strain rate is low (S2-1-0.23), the large blocks are prominent. Specifically, specimen S2-1-0.25 shows minor local failures, but with the increase of the strain rate, the specimen becomes almost completely crushed.

Figure 10 also illustrates the bar chart of the mass percentage distribution of fragments with different particle sizes. Most of the mass is represented by fragments with particle sizes greater than 5 mm. For the cyan sandstone, the corresponding relationship between the mass proportion of the fragments and the strain rate is pronounced. The mass proportion of coarse (larger than 5 mm) fragments decreases with the increase of the strain rate, while the percentage of fine fragments (<5 mm) increases with the increment of the strain rate.

Additionally, the fractal dimension (FD) of the fragments can also reflect the fragmentation characteristics. In
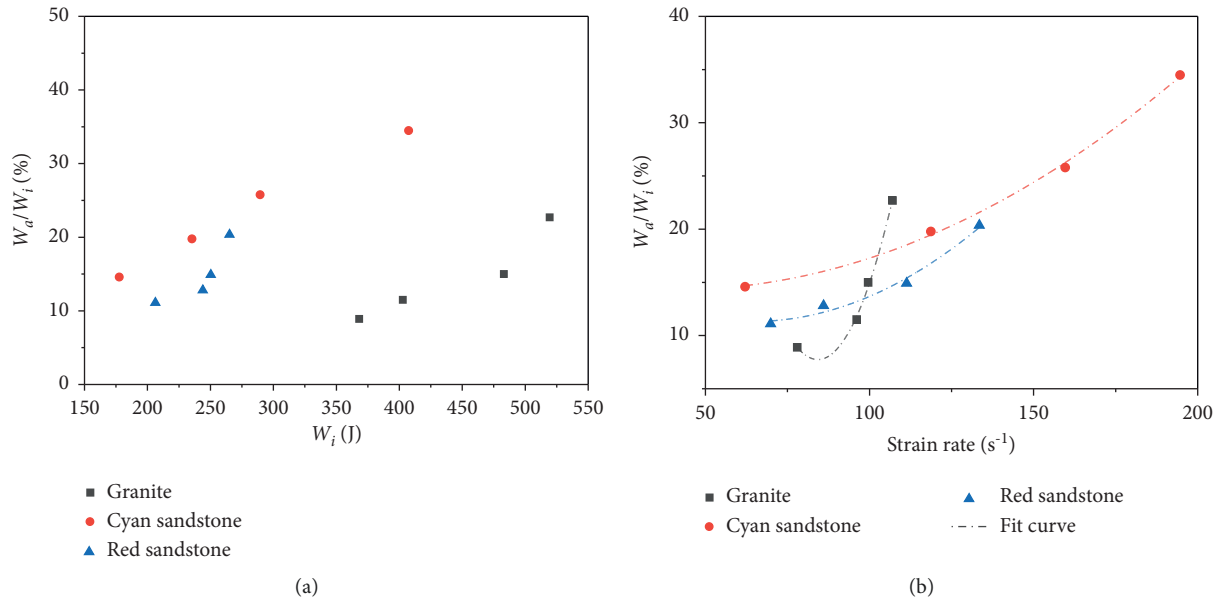
FIGURE 9: Variations of energy absorption rate versus (a) incident energy and (b) strain rate.
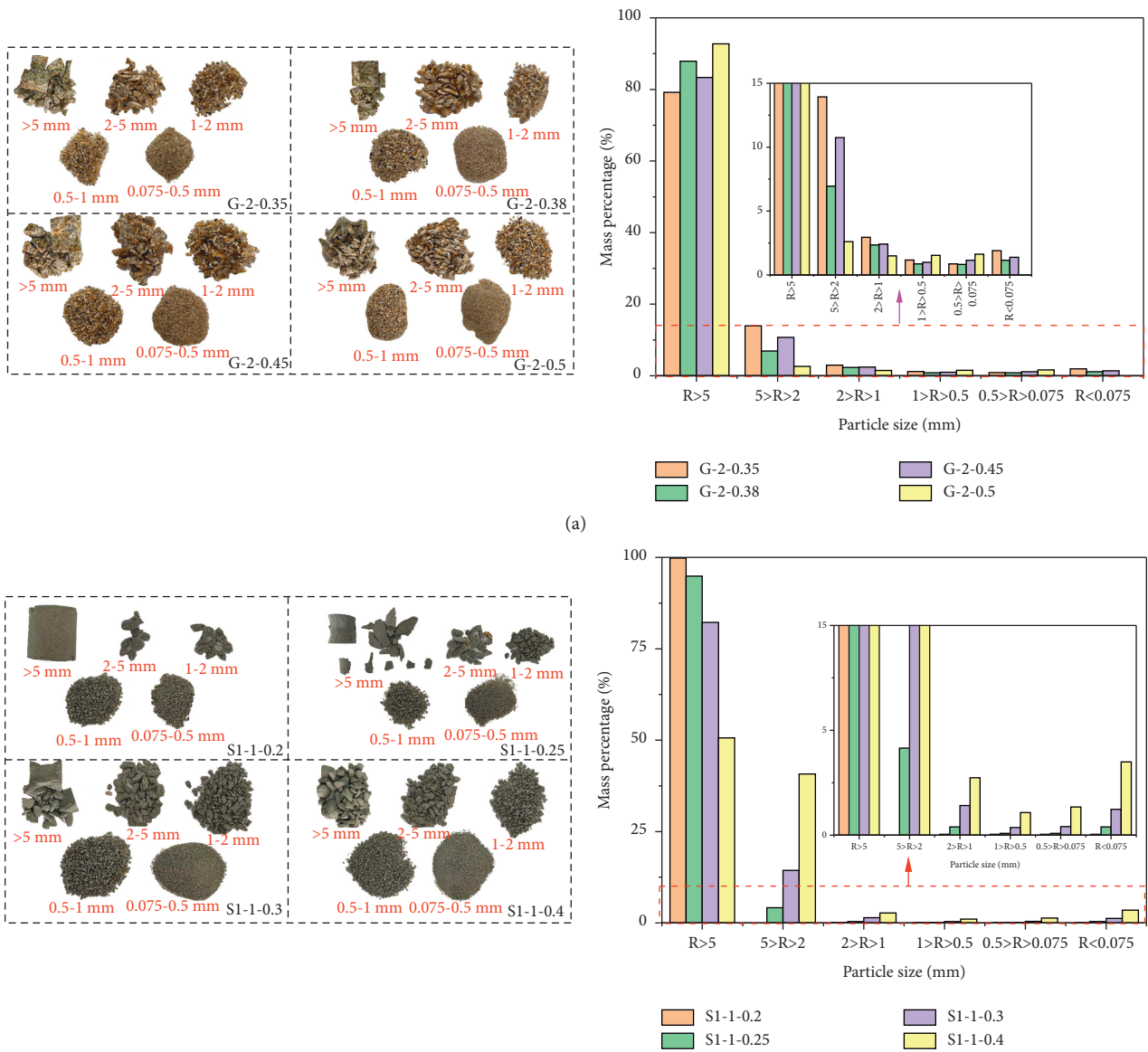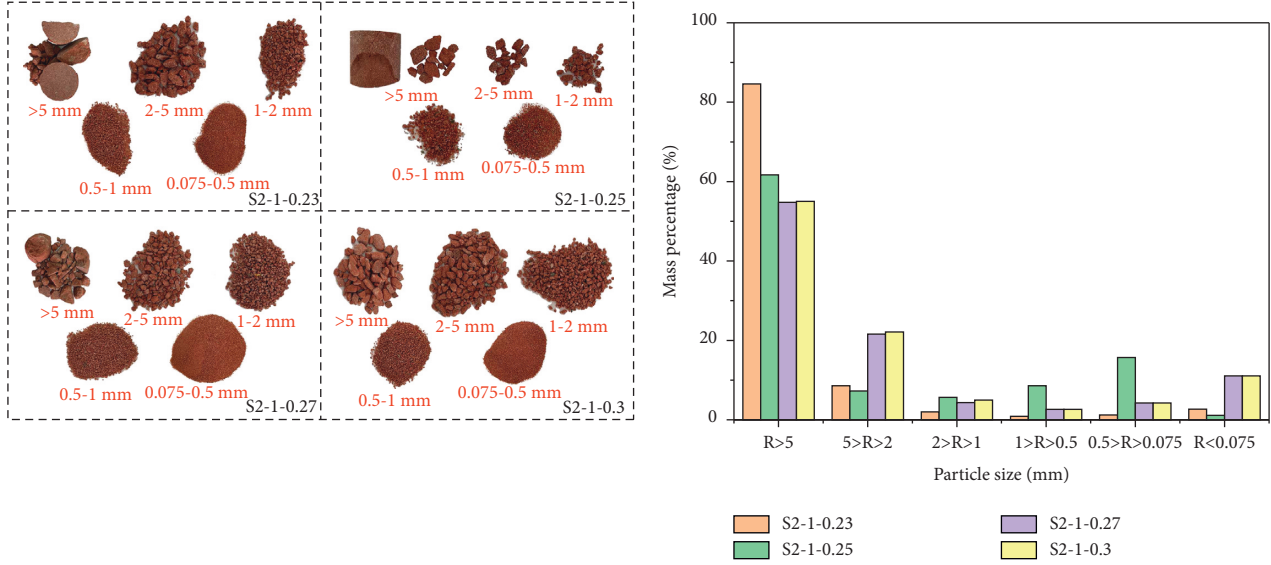

(a)

(b)

FIGURE 10: Continued.

(c)

FIGURE 10: Fragments and the corresponding mass percentage of (a) granite, (b) cyan sandstone, and (c) red sandstone after different strain rate loadings.

this article, the FD uses the particle size-number calculation method [37]. The fragments (particle sizes greater than 5 mm) were equated with a cube, and based on the measured length (l), width (w), and thickness (h) of the fragments (the above three values were the maximum values in the three directions), the equivalent edge length L_{eq} of the cube was calculated, while the corresponding FD was determined according to the following equation:

$$N = N_0 \left(\frac{L_{eq}}{L_{eqmax}} \right)^{-D},$$ (6)

where L_{eq} equals $(l \times w \times h)^{1/3}$; N is the number of fragments in the selected scale less than L_{eq}; N_0 is the number of fragments corresponding to the L_{eqmax}; D is the FD value. When $\lg(L_{eqmax}/L_{eq})$ and $\lg N$ are considered as the horizontal and the vertical coordinates, respectively, the slope of the fitting straight line is the FD, as illustrated in Figures 11(a). Figure 11(b) indicates the variation of the FD with the strain rate. The variation laws of the different lithological types are consistent; therefore, the FD values show a positive correlation with the strain rate. Additionally, the increase process of the FD values for the granite and the cyan sandstone increases almost linearly, while the values for red sandstone suggest a nonlinear growth process. Due to the wide-ranging interval of the strain rate in the case of the cyan sandstone, the increase of the FD has the smallest values (2.1–3.1), while the increase in the case of the granite is the most noticeable, followed by the red sandstone. The growth rate of the FD values of the red sandstone is slow within a range of the strain rate, but it rapidly increases after exceeding a certain critical value. In general, higher FD

values result in the generation of more small-sized fragments.

3.2. Drilling Properties

3.2.1. Drilling Characteristics. The drilling curve can be used to quantitatively evaluate the drilling process under different values of the DP and the RS. Figure 12 illustrates the drilling curves of the red sandstone with a DP value equal to 60 N and different RSs, with the final drilling depth reaching 20 mm. As shown in Figure 12, the drilling processes under different RSs are similar and can be divided into two stages: the initial drilling stage and the uniform drilling stage. During the initial drilling stage, the drilling depth of the bit is shallow, and the bit is near the initial position. Because the cuttings produced by the interaction between the bit and the rock are easier to be discharged, the drilling resistance of the bit is relatively small, while the DS is faster and less influenced by the RS. During the second uniform drilling stage, the drilling depth of the boundary point between the two stages is located at approximately 3 mm for the red sandstone sample. After entering the second stage, the resistance of the cuttings around the bit has an impact on the DS, and with the increase of the drilling depth, the impact is mostly consistent. Specifically, the DS remains basically unchanged, but it is affected by the RS of the drilling rig. Higher RS values cause higher DS values. Additionally, when the RS is low, the drilling curves (700 r/min and 900 r/min) indicate distinct fluctuations and when the drilling depth reaches a certain value, the fluctuation gradually decreases. Moreover, for the cyan sandstone and the granite, the curves of the
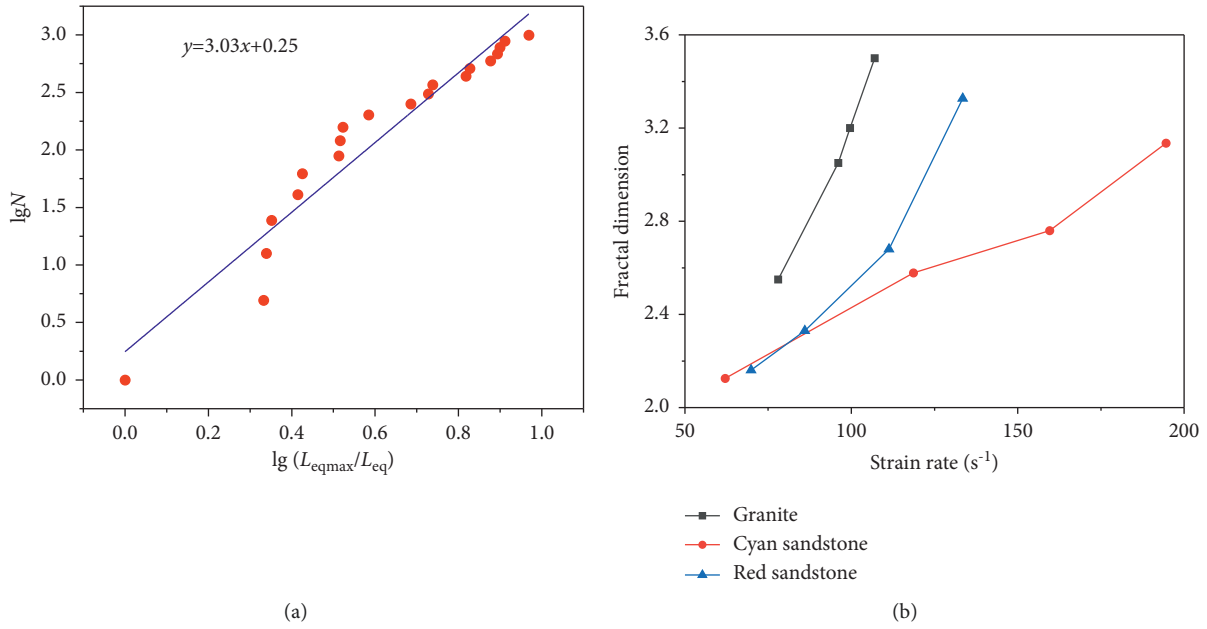
FIGURE 11: (a) Diagram of FD calculation and (b) variations of the FD with the strain rate.
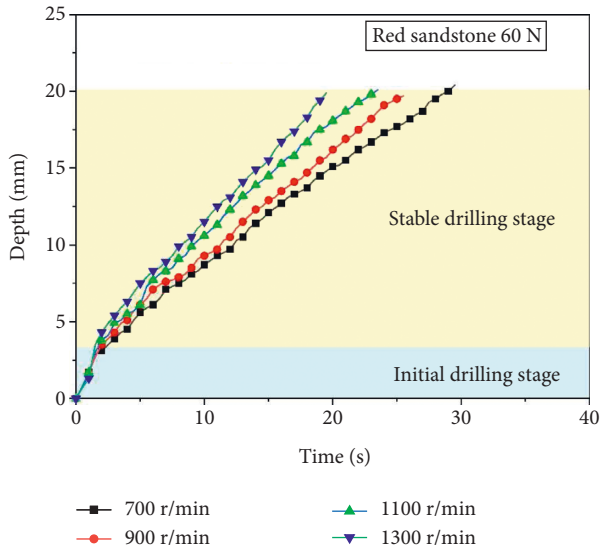

FIGURE 12: The variation of the drilling depth with time for the red sandstone under different RS (DP = 60 N).

drilling process are generally consistent with those of the red sandstone, but there is a significant difference in the drilling time and the drilling rate.

3.2.2. Influence of the Drilling Pressure and the Revolution Speed. According to the drilling tests of the different lithological samples, the slope of the drilling curve in the stable drilling stage was selected as the reference DS. The variation curves of the DS of the granite, cyan sandstone, and red sandstone samples under the same DP with different RSs and the same RS with different DPs were plotted in Figures 13–15, respectively. Table 3 lists the obtained values.

Overall, the influence of the sample RS and DP of different lithologies on the DS is consistent, with an increase in the DP or the RS causing an acceleration of the DS. For the granite, when the DP has lower values (250 N), the increase of the RS is more noticeable than the increase in the DS. Hence, in comparison with the DP increment, the increase of the RS has a minor effect on the growth of the DS. On the other side, when the RS is constant, the increase of the DP has an invariable influence on the improvement of the DS, and the overall improved efficiency is higher than the one derived from the RS. Particularly, the influence of the DP on the DS in the case of the granite is more evident.

For the cyan sandstone characterized by medium strength values, the increase of the DP is also more efficient than the increase of the RS. Specifically, when the RS remains constant and the DP is higher, the increment of the DS with the increase of the DP is more distinct. For example, when the DP is raised from 50 N to 60 N, the DS increases by approximately 25.8%, while the increment is the same at different RSs. When the DP has the same values, the increase of the RS has little effect on the increase of the DS, with an average increment equal to 11.1%. The values of the DP and the RS selected for the red sandstone are similar to those used for the cyan sandstone, but because the strength of the red sandstone is lower, the DS values are generally higher than the DS values of the cyan sandstone. Specifically, when the DP is higher (60 N), the increase of the DS (about 26.4%) is more noticeable with the increase of the RS. Similarly, when the RS is greater, the increase of the DS is also more evident with the increase of the DP. For example, when the RS is equal to 1300 r/min, the maximum increment can reach 57%.

3.3. Energy Consumption of the SHPB and the Drilling Tests. For the SHPB test, the energy consumption of the sample can be quantitatively characterized by the dissipation energy
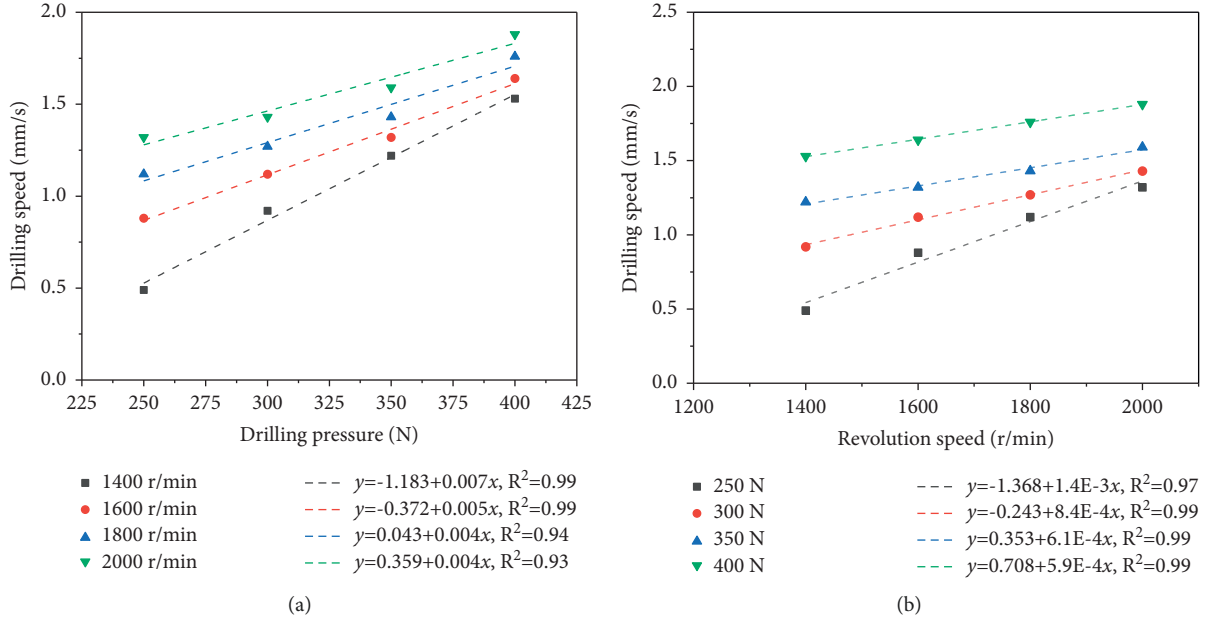
(a)

(b)

FIGURE 13: The variations of the DS with (a) the DP and (b) the RS of granite.
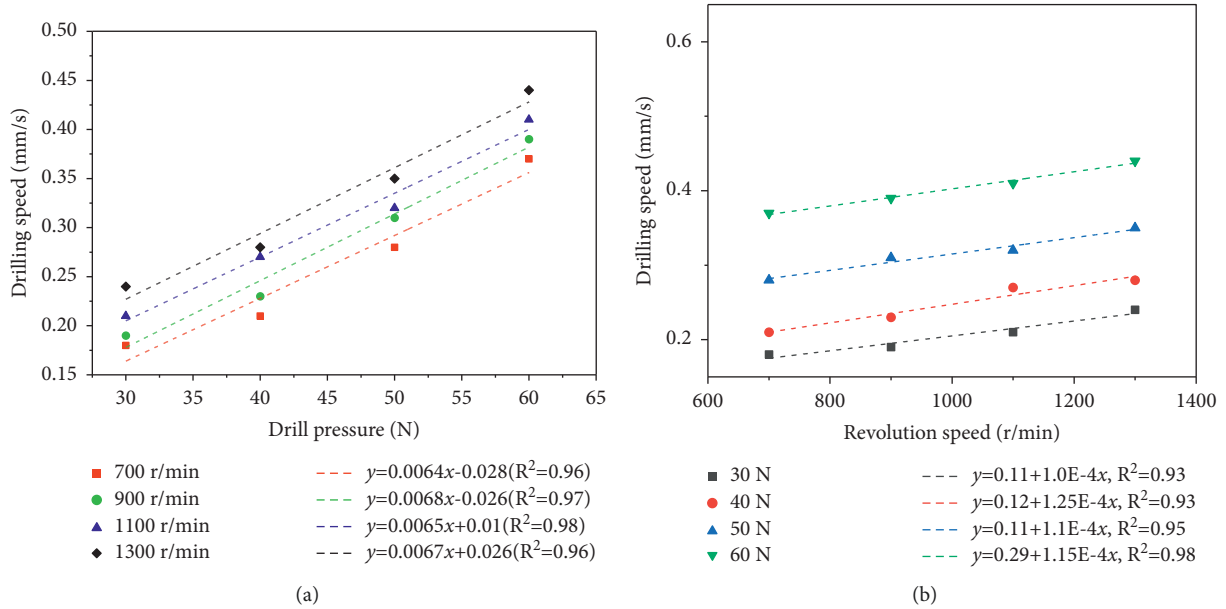

(a)

(b)

FIGURE 14: The variations of the DS with (a) the DP and (b) the RS of cyan sandstone.

density. This describes the dissipation energy per unit of volume (equation (7)) [38], which in physical meaning terms represents the energy consumed during the rock crushing process of one unit of volume. Additionally, the dissipation energy density (η) values of the samples with different lithologies are listed in Table 2. For the drilling test, the mechanical specific energy (MSE) of the drilling process can be obtained based on the MSE theory (equation (8)), and the bit torque from the formula can be calculated according to

equation (9). Thus, the MSE represents the energy required to crush one unit of volume.

$$\eta = \frac{W_a}{V}, \tag{7}$$

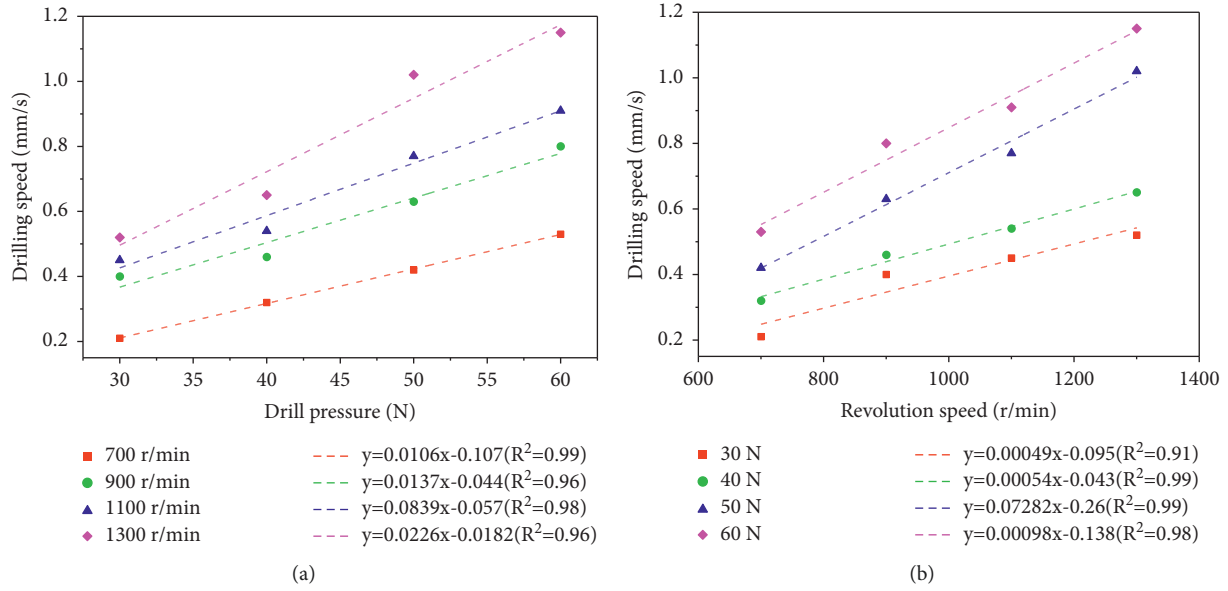$$M = \frac{4W}{\pi D_b^2} + \frac{480 r T_b}{D_b^2 R}. \tag{8}$$

(a)

(b)

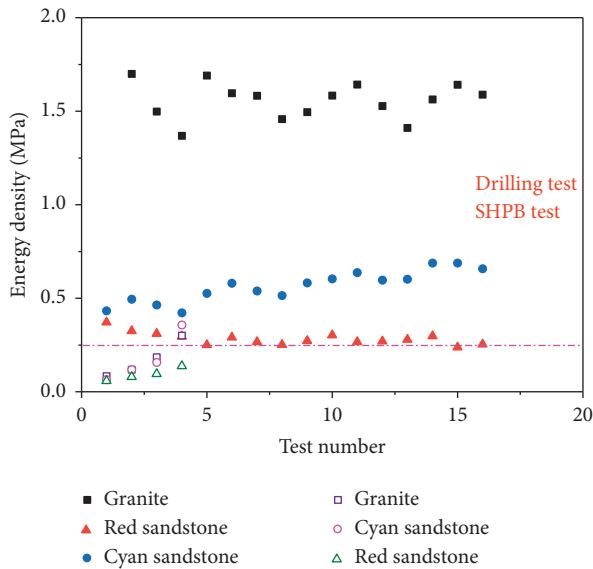FIGURE 15: The variations of the DS with (a) the DP and (b) the RS of red sandstone.

FIGURE 16: The scatters of the MSE and the energy density of the drilling and SHPB tests.

$$T_b = 0.000333\mu W D_b, \tag{9}$$

where V is the sample volume, mm^3; M is the MSE, MPa; W is the DP, kN; D_b is the bit diameter, mm; r is the RS, r/min; T_b is the bit torque, kN·m; R is the DS, m/h; μ is the specific sliding friction coefficient of the drill bit, which in this article is equal to 0.5.

Therefore, η of the SHPB test has the same physical significance as the MSE of the drilling test. Figure 16 illustrates the scatter plot between η and the MSE derived from the different lithological samples. Overall, the energy required to crush one unit of volume during the drilling test procedure is higher than during the dynamic impact test.

Additionally, the MSE of the samples with different lithologies is correlated with the strength of the samples, which means that higher strength values correspond to higher MSE values. Moreover, in terms of the drilling process, the broken rock mass mainly uses the extrusion and the cutting effect of the bit on the rock. The shear resistance of the rock represents the main source of energy dissipation, and the frictional heating generated during the drilling process will also dissipate some of the energy. However, for the dynamic impact test, the propagation of tensile stress waves in the sample creates several tensile cracks in the rock, which eventually leads to the generation of fractures. As it is known, the tensile performance of rocks is significantly lower than the shear resistance, so the MSEs values of the drilling test are high. Therefore, to optimize the blasting design using the drilling parameters of the bench borehole drilling process, it is necessary to establish the corresponding relationship between the energy consumption of drilling and blasting rock processes according to the field measured data.

4. Conclusion

To analyze the variations in energy consumption of different rock crushing methods, this study performed SHPB and drilling tests on three lithologies of rocks. The dynamic impact crushing characteristics were analyzed based on the dynamic stress-strain curve, the peak stress, the energy, and failure mode, while the drilling crushing characteristics were analyzed based on the drilling curve and the influence of the DP and the RS on the DS. Finally, the energy consumption differences between the two methods were compared. The main conclusions are as follows:

(1) The sensitivity of the dynamic strength of rocks with different lithologies to strain rate is different. When the UCS values are higher, the increase of the strain rate has a prominent contribution to the

strengthening of the peak stress, while lower UCS values indicate that the plastic characteristics of the dynamic stress-strain curves are more evident.

(2) The EUE of the dynamic impact test sample has a positive correlation with the strain rate. Higher EUE values are associated with a higher proportion of fine fragments and an increase of the FD of coarse fragments.

(3) The typical drilling process can be divided into two stages: initial drilling and stable drilling. The drilling speed in the stable drilling stage is lower than in the initial drilling stage. Additionally, the DP and the RS indicate a positive linear correlation with the DS, and the influence of the DP on the DS is more pronounced.

(4) The energy consumption required to crush one unit of volume during the drilling process is higher than the energy consumption during the dynamic impact.

Data Availability

All data used during the study are available from the corresponding author by request.

Conflicts of Interest

The authors declare that there are no conflicts of interest in this work.

Acknowledgments

References

[1] Z. Yan, F. Dai, and Y. Liu, "Dynamic strength and cracking behaviors of single-flawed rock subjected to coupled static-dynamic compression," *Rock Mechanics and Rock Engineering*, vol. 53, no. 9, pp. 4289–4298, 2020.

[2] X. S. Li, Q. H. Li, and Y. J. Hu, "Study on three-dimensional dynamic stability of open-pit high slope under blasting vibration," *Lithosphere*, vol. 2022, Article ID 6426550, 17 pages, 2019.

[3] D. H. Chen, H. Chen, W. Zhang, J. Q. Lou, and B. Shan, "An analytical solution of equivalent elastic modulus considering confining stress and its variables sensitivity analysis for fractured rock masses," *Journal of Rock Mechanics and Geotechnical Engineering*, 2021.

[4] Q. Wang, M. C. He, S. C. Li et al., "Comparative study of model tests on automatically formed roadway and gob-side entry driving in deep coal mines," *International Journal of Mining Science and Technology*, vol. 31, no. 4, pp. 591–601, 2021.

[5] K. Ma and G. Liu, "Three-Dimensional discontinuous deformation analysis of failure mechanisms and movement characteristics of slope rock falls," *Rock Mechanics and Rock Engineering*, vol. 55, no. 4, pp. 1–22, 2022.

[6] C. Zhu, M. Karakus, M. C. He et al., "Olumetric deformation and damage evolution of Tibet interbedded skarn under multistage constant-amplitude-cyclic loading," *International Journal of Rock Mechanics and Mining Sciences*, vol. 152, 2022.

[7] Y. Wang, H. N. Yang, J. Q. Han, and C. Zhu, "Effect of rock bridge length on fracture and damage modelling in granite containing hole and fissures under cyclic uniaxial increasing-amplitude decreasing-frequency (CUIADF) loads," *International Journal of Fatigue*, vol. 158, 2022.

[8] Y. Q. Su, F. Q. Gong, S. Luo, and Z. X. Liu, "Experimental study on energy storage and dissipation characteristics of granite under two-dimensional compression with constant confining pressure," *Journal of Central South University*, vol. 28, no. 3, pp. 848–865, 2021.

[9] G. Li, Y. Hu, S. M. Tian, W. B. Ma, and H. L. Huang, "Analysis of deformation control mechanism of prestressed anchor on jointed soft rock in large cross-section tunnel," *Bulletin of Engineering Geology and the Environment*, vol. 80, pp. 9089–9103, 2021.

[10] C. Cao, W. Zhang, J. Chen, B. Shan, S. Song, and J. Zhan, "Quantitative estimation of debris flow source materials by integrating multi-source data: a case study," *Engineering Geology*, vol. 291, Article ID 106222, 2021.

[11] K. Peng, Z. P. Liu, and Q. L. Zou, "Static and dynamic mechanical properties of granite from various burial depths," *Rock Mechanics and Rock Engineering*, vol. 52, pp. 3545–3566, 2019.

[12] X. B. Li, Y. Zou, and Z. L. Zhou, "Numerical simulation of the rock SHPB test with a special shape striker based on the discrete element method," *Rock Mechanics and Rock Engineering*, vol. 47, no. 5, pp. 1693–1709, 2013.

[13] Y. Xu, F. Dai, N. W. Xu, and T. Zhao, "Numerical investigation of dynamic rock fracture toughness determination using a semi-circular bend specimen in split Hopkinson pressure bar testing," *Rock Mechanics and Rock Engineering*, vol. 49, no. 3, pp. 731–745, 2016.

[14] B. Lundberg, "A split Hopkinson bar study of energy absorption in dynamic rock fragmentation," *International Journal of Rock Mechanics and Mining Sciences & Geomechanics Abstracts*, vol. 13, no. 6, pp. 187–197, 1976.

[15] Z. Y. Liao, J. B. Zhu, K. W. Xia, and C. A. Tang, "Determination of dynamic compressive and tensile behavior of rocks from numerical tests of split Hopkinson pressure and tension bars," *Rock Mechanics and Rock Engineering*, vol. 49, no. 10, pp. 1–18, 2016.

[16] F. S. Boukredera, A. Hadjadj, and M. R. Youcefi, "Drilling vibrations diagnostic through drilling data analyses and visualization in real time application," *Earth Science India*, vol. 14, no. 4, pp. 1–18, 2021.

[17] Z. Dou, S. X. Tang, X. Y. Zhang et al., "Influence of shear displacement on fluid flow and solute transport in a 3D rough fracture," *Lithosphere*, vol. 2021, 2021.

[18] P. Zhang, D. F. Zhang, Y. Yang et al., "Study on integrated modeling of spatial information of a complex geological body," *Lithosphere*, vol. 2022, 2022.

[19] W. C. Sanstrom and M. J. Hawkins, "Perceiving drilling learning through visualization," in *Proceedings of the IADC/ SPE Asia Pacific Drilling Technology Conference, APDT*, Limerick, Ireland, September 2000.

[20] D. Cao, C. Loesel, and S. Paranji, "Rapid development of real-time drilling analytics system," in *Proceedings of the IADC/ SPE Drilling Conference and Exhibition Conference*, Fort Worth, TX, USA, March 2018.

[21] D. F. Howarth and J. C. Rowlands, "Quantitative assessment of rock texture and correlation with drillability and strength

properties," *Rock Mechanics and Rock Engineering*, vol. 20, no. 1, pp. 57–85, 1987.

[22] C. R. Lakshminarayana, A. K. Tripathi, and S. K. Pal, "Experimental investigation on potential use of drilling parameters to quantify rock strength," *International Journal of Geo-Engineering*, vol. 12, 2021.

[23] M. Henry, T. Abbas, and C. Emmanuel, "Rock drilling performance evaluation by an energy dissipation based rock brittleness index," *Rock Mechanics and Rock Engineering*, vol. 49, no. 8, pp. 3343–3355, 2016.

[24] C. H. Song, K. B. Kwon, M. G. Cho, J. Y. Oh, D. Y. Shin, and J. W. Cho, "Development of lab-scale rock drill apparatus for testing performance of a drill bit," *International Journal of Precision Engineering and Manufacturing*, vol. 16, pp. 1405–1414, 2015.

[25] J. Chen and Z. Q. Yue, "Ground characterization using breaking-action-based zoning analysis of rotary-percussive instrumented drilling," *International Journal of Rock Mechanics and Mining Sciences*, vol. 75, pp. 33–43, 2015.

[26] S. Kahraman, N. Bilgin, and C. Feridunoglu, "Dominant rock properties affecting the penetration rate of percussive drills," *International Journal of Rock Mechanics and Mining Sciences*, vol. 40, no. 5, pp. 711–723, 2003.

[27] S. C. Li, B. Liu, X. J. Xu et al., "An overview of ahead geological prospecting in tunneling," *Tunnelling and Underground Space Technology*, vol. 63, pp. 69–94, 2017.

[28] Q. Wang, H. K. Gao, H. C. Yu, B. Jiang, and B. H. Liu, "Method for measuring rock mass characteristics and evaluating the grouting-reinforced effect based on digital drilling," *Rock Mechanics and Rock Engineering*, vol. 52, no. 1, pp. 841–851, 2019.

[29] M. Mostofi, V. Rasouli, and E. Mawuli E, "An estimation of rock strength using a drilling performance model: a case study in Blacktip field, Australia," *Rock Mechanics and Rock Engineering*, vol. 44, no. 3, pp. 305–316, 2011.

[30] J. Hamelin, J. Levallois, and P. Pfister, "Enregistrement des parameters de forage: nouveaux developments," *Bulletin of the International Association of Engineering Geology-Bulletin de l'Association Internationale de Géologie de l'Ingénieur*, vol. 26, pp. 83–88, 1982.

[31] P. Pfister, "Recording drilling parameters in ground engineering," *Ground Engineering*, vol. 18, no. 3, pp. 16–21, 1985.

[32] Q. Wang, H. K. Gao, B. Jiang, J. Yang, and Z. J. Lv, "Relationship model for the drilling parameters from a digital drilling rig versus the rock mechanical parameters and its application," *Arabian Journal of Geosciences*, vol. 11, 2018.

[33] B. Huang, W. Y. Guo, Z. Y. Fu, T. B. Zhao, and L. S. Zhang, "Experimental investigation of the influence of drilling arrangements on the mechanical behavior of rock models," *Geotechnical & Geological Engineering*, vol. 36, no. 4, pp. 2425–2436, 2018.

[34] M. He, N. Li, Z. Q. Zhang, X. C. Yao, Y. S. Chen, and C. H. Zhu, "An empirical method for determining the mechanical properties of jointed rock mass using drilling energy," *International Journal of Rock Mechanics and Mining Sciences*, vol. 116, no. 4, pp. 64–74, 2019.

[35] T. Wang and B. Shang, "Three-wave mutual-checking method for data processing of SHPB experiments of concrete," *Journal of Mechanics*, vol. 30, no. 5, pp. 5–10, 2014.

[36] Z. Zhang, S. Kou, L. G. Jiang, and P. Lindqvist, "Effects of loading rate on rock fracture: fracture characteristics and energy partitioning," *International Journal of Rock Mechanics and Mining Sciences*, vol. 37, no. 5, pp. 745–762, 2000.

[37] Y. Wang, C. Zhu, M. C. He, and D. Q. Liu, "Fragmentation characteristics analysis of sandstone fragments for impact rockburst under different dynamic loading frequency," *Geotechnical & Geological Engineering*, vol. 37, no. 44, pp. 2715–2727, 2019.

[38] W. J. Liu, K. Yang, W. Zhen, X. L. Chi, R. J. Xu, and X. Lv, "Energy dissipation and failure characteristics of layered composite rocks under impact load," *Shock and Vibration*, vol. 2021, Article ID 8775338, 14 pages, 2021.